ELM Suppression in DIII-D Hybrid Plasmas Using *n*=3 Resonant Magnetic Perturbations

B. Hudson[1], T.E. Evans[2], T.H. Osborne[2], C.C. Petty[2], and P.B. Snyder[2]

[1]Oak Ridge Institute for Science Education, Oak Ridge, Tennessee 37831, USA
[2]General Atomics, P.O. Box 85608, San Diego, California 92186-5608, USA

e-mail: hudson@fusion.gat.com

Abstract. Experiments performed at the DIII-D tokamak have successfully demonstrated complete suppression of edge localized modes (ELMs) in the hybrid scenario via the application of a resonant magnetic perturbation (RMP). These high confinement (H98y2 > 1) discharges, with a shape similar to that planned for ITER, have pressure gradients in the edge that are believed to drive a parallel bootstrap current which is dominant over other current sources in this region. Steep pressure and current gradients can cause unstable MHD modes known as peeling-ballooning (PB) modes and are thought to drive large "Type-I" ELMs typical in the tokamak H-mode. Peeling-ballooning stability calculations, performed with the ELITE code, are dependent on both the edge pressure and current gradients and show that the ELM suppressed hybrid discharges are stable. It was also determined that the EPED1 code, which has successfully been used to predict the total pedestal height in standard ELMing H-mode discharges across a number of different machines, is in general agreement with the hybrid discharges analyzed here. Additionally, the inclusion of the edge bootstrap current has a non-negligible effect on the determination of magnetic field line stochasticity in the pedestal region; the driving mechanism behind RMP.

1. Introduction

The success of the technique known as resonant magnetic perturbation (RMP) [1–7] in suppressing Type I edge-localized modes (ELMs) [8] in fusion plasmas continues to motivate the study of this physics with a wide range of plasma conditions that could be used in ITER or other burning plasmas. The "hybrid" scenario [9,10] was developed on DIII-D to be an intermediate step between the standard high-current, high-confinement (H-mode) scenario [11] and the steady-state advanced tokamak scenario [12]. Hybrids are referred to as "high-performance" as they typically operate with H-factors (H98y2 scaling) of > 1 (H98y2 = 1 is the ITER baseline). They are considered "stationary" because the discharges maintain nearly constant confinement for several current diffusion times.

The hybrid scenario is characterized by having a modest plasma current and maintaining high β_N (>2.2), where $\beta_N = P/(B^2/2\mu_0)/(I/aB_T)$, which is the ratio of the plasma pressure, P, to the magnetic pressure normalized I/aB_T. Here B is the total magnetic field, B_T the toroidal magnetic field, I the plasma current and a is the minor radius. The safety factor, q, $q = d\Phi/d\psi$, where Φ is the toroidal flux and ψ is the poloidal flux, is kept above unity to stabilize the sawtooth instability [13,14]. The values of β_N, typical of hybrid discharges, and the low transport levels characteristic of the H-mode pedestal region, result in large pressure and current gradients the plasma edge. These gradients are thought to be the source of free energy to drive instabilities known as peeling-ballooning (P-B) modes [15,16]. The peeling mode is driven by current gradients and the ballooning mode is driven by pressure gradients. In the pedestal, the two gradients are coupled through the bootstrap current [17–19], which is a neoclassical pressure gradient driven current. To suppress the ELMs typical of H-mode plasmas, a magnetic perturbation normal to the flux surfaces is introduced that is believed to render the magnetic topology in the plasma edge partially stochastic. In poloidally diverted plasmas, such as DIII-D, stochastic magnetic field lines connect the pedestal plasma just inside the separatrix to the divertor target plates forming 'open' field lines. Heat and particle

transport is expected to be larger along the open field lines, reducing the edge pressure gradient and stabilizing the ELMs.

Recent experiments on DIII-D demonstrated the complete suppression of ELMs in hybrid discharges using $n = 3$ RMP [20]; an investigation of the physics behind this suppression and a comparison with the standard H-mode regime was undertaken in [21]. This paper continues that analysis with an additional emphasis on the role of bootstrap current on the magnetic topology of high-beta plasmas, relevant to the hybrid or other high-performance regimes.

2. ELM Suppression in Hybrid Plasmas

The DIII-D tokamak is a toroidal confinement device, major radius R = 1.7 m, minor radius a = 0.6 m. For the discharges discussed here, the toroidal magnetic field B_T, ranged from 1.5 to 2.1 T, and plasma current I_p ranged from 1.2 MA to 1.5 MA. For typical H-mode plasmas β_N = 1.0–2.0 and q_{95} ranges from 3–6. In the hybrid scenarios discussed in this paper, β_N = 2.0 – 2.5, q_{95} = 3–4, with a single X-point just above the lower diverter. We begin with an example of ELM suppression by RMP in a hybrid plasma. ELM suppression is believed to be achieved by rendering the plasma edge stochastic and using the increased particle and heat transport to suppress pressure and current gradient driven instabilities. This is done by increasing non-axisymmetric magnetic field normal to the flux surfaces, at rational q surfaces in the plasma edge that are resonant with the toroidal mode number of the perturbation. An array of upper and lower coils which approximate saddle loops (Fig. 1), referred to as "I-coils" [22,23], accomplish this task by generating a significant radial field component when current is applied. There are six coils in the toroidal direction above the midplane and six below the midplane. This allows up to an $n = 3$ perturbation to be imposed on the plasma. When the currents in the upper and lower I-coils at a particular toroidal angle flow in the same direction (δB in the same into or out of the plasma for both) this called "even-parity". When the coil currents are in opposite directions (δB into the plasma for the upper coil, and out of the plasma for the lower coil, or vice-versa) this is called "odd parity". All experiments described in this paper were done in even parity, which has been shown to maximize the resonant component of the applied perturbation. The large q shear in the edge results in overlapping islands for closely spaced $n = 3$ resonant surfaces (8/3, 9/3, 10/3, 11/3, etc.), excluding any response of the plasma due to these resonant islands. This is believed to increase transport in the edge and lower the pressure gradient, which should lead to ELM stabilization based on P-B theory.

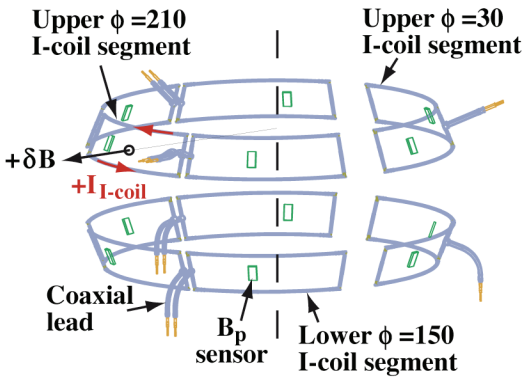

FIG. 1. The I-coil comprises six segments above the equatorial plane (upper) and six segments below (lower) [3].

2.1. Comparison to Standard H-mode

The suppression of ELMs in a hybrid plasma, 129949, is shown in Fig. 2 and compared to an RMP ELM suppressed plasma in a standard H-mode, 125606. The relevant plasma parameters for the hybrid were: B_T = 1.5 T, I_p = 1.2 MA, β_N = 2.5. The most common diagnostic to identify ELMs are filterscopes [24], which are narrow wavelength optical filters that are tuned to detect D_α light [Fig. 2(a)]. Emission increases during ELMs due to increases in electron impact-excitation from plasma-wall interactions. There is also an increase in the baseline emission in the RMP phase, which is consistent with a higher outward particle flux, associated with the increased particle transport. ELMs in the hybrid discharge return around

3500 ms due to the onset of a 3/2 mode [Fig. 2(b)] that locks to the vessel wall and stops the plasma rotation [Fig. 2(c)], with a disruption following at 4000 ms. It has been observed that ELM suppression is lost at low rotation, typically < 40 km/s, though the physics behind it is not yet understood. Figure 2(d) compares the typical plasma currents for an H-mode (B_T = 1.9 T) and a hybrid (B_T = 1.5 T). The distinction between standard H-mode and the "hybrid" is that hybrids have a saturated core mode (usually a 3/2 NTM) resulting in excellent confinement (H98y2 = 1.4). In Fig. 2(e), β_N during RMP is about 90% of the pre-RMP value despite a 10% increase in the injected power through additional neutral beam sources using β feedback control. The value of q_{95} [Fig. 2(f)], defined as q at 95% poloidal flux surface, is controlled to be fairly constant, and at approximately 3.6. In RMP discharges an empirical "q_{95} resonance window" is observed where q_{95} must be within in order for complete ELM suppression to occur. The resonance window has been found to be dependent on the plasma shape, described partially in terms of triangularity, δ and elongation, κ. For a standard H-mode (δ_{lower} = 0.73, δ_{upper} = 0.35, and κ = 1.76), q_{95} was scanned to observe the range required for complete ELM suppression. The resulting window for ELM suppression was found to be 3.5 < q_{95} < 3.9 [6]. The shape parameters for the hybrid were δ_{lower} = 0.7, δ_{upper} = 0.36, and κ = 1.82.

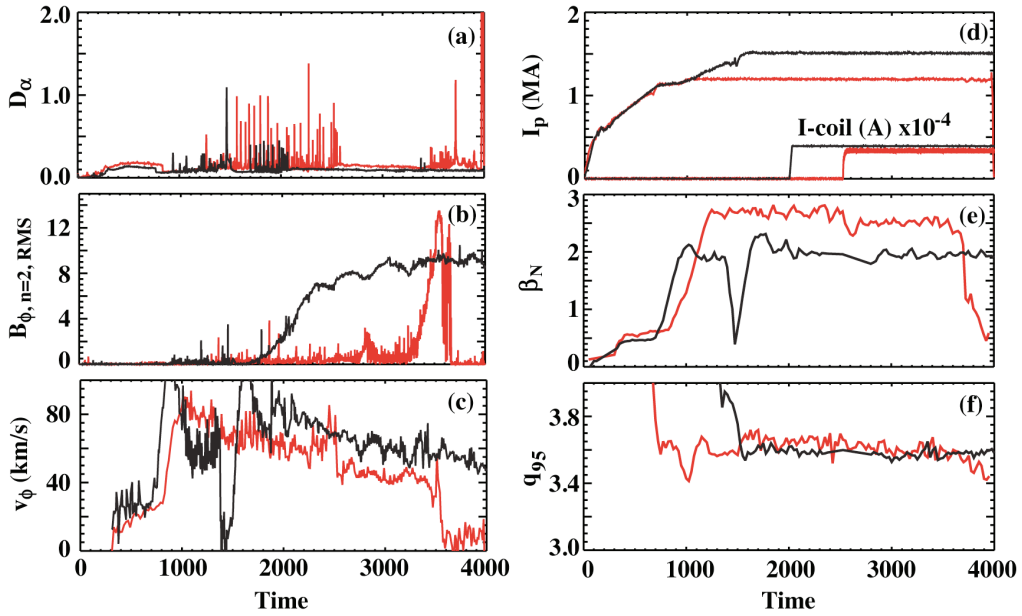

FIG. 2. ELM suppression in a typical H-mode (black) discharge and a hybrid (red) discharge. (a) D_α light indicates the presence of ELMs and shows suppression during RMP. (b) RMS $n=2$ magnetic mode amplitude. (c) Pedestal toroidal rotation velocity. (d) I_p and I-coil current. (e) β_N. (f) q_{95} [21].

2.2. Peeling-Ballooning Stability

The stability to P-B modes is examined for a hybrid discharge with nearly 1 s of RMP ELM suppression, shot 129949. We utilize the ELITE [25] code to determine the normalized growth rates of the edge modes that drive ELMs. The mode growth rate is dependent on the edge pressure and current gradients. To determine the pressure profile, Thomson scattering [26] (n_e,T_e), CER [27] (n_i,T_i) is used. The measurements for the ELMing phase before RMP are averaged between 1500 and 2500 ms. A specific level for the D_α signal is assumed to constitute a Type I ELM, to distinguish them from the noise or other small ELMs. The data for n_e, T_e, n_i, T_i, for the pressure profile construction is taken during the last 20% of the large-ELM periods. This is to have profiles that are reflective of the unstable pressure gradients that lead to ELMing, as opposed to profiles that may be in flux or relaxed due to the

occurrence of an ELM. During the phase of RMP ELM suppression, a 200 ms averaging window was used. The ONETWO [28] code is used to calculate the fast ion pressure.

Equilibrium reconstruction of shot 129949 shows a decrease in the edge current gradient [Fig. 3(a)] and pressure gradient [Fig. 3(b)] by about a factor of two after RMP is applied at t = 2500 ms. As a result, the plasma that was initially unstable to P-B modes before RMP [Fig. 4(a)] is moved to a stable region of α, J' space after RMP is applied [Fig. 4(b)] according to ELITE calculations (note that the P-B stability boundaries also change when the RMP is applied). The uncertainty in the J' value is estimated by minimization of χ^2 during equilibrium reconstruction. The relationship between P-B stability and ELM suppression has also been applied to standard H-mode plasmas at lower β_N [5–7].

2.3. q_{95} Resonance Window

As with the case of H-mode plasmas a resonant window in q_{95} for ELM suppression by RMP was observed in hybrid plasmas. We compare the two hybrid discharges, 129949, with a q_{95} of 3.6 during RMP and 129972 with a q_{95} of 4.1 during RMP. The toroidal field, B_T, was ramped up in 129972 after 1 s, in order to raise q. The ELMs are not suppressed in the q_{95} = 4.1 case [Fig. 5(a)] even though the change in β_N [Fig. 5(b)] is similar. The plot of q_{95} is shown in Fig. 5(c).

Before RMP was applied, ELITE showed that both shots were unstable to Type I ELMs, which were observed experimentally. After RMP was applied, shown in Fig. 6(a,b), there was a decrease in the plasma current and pressure gradients, with P' and J' having similar maximum values for the two shots. However, during RMP, the pedestal width for the q_{95} = 4.1 case is

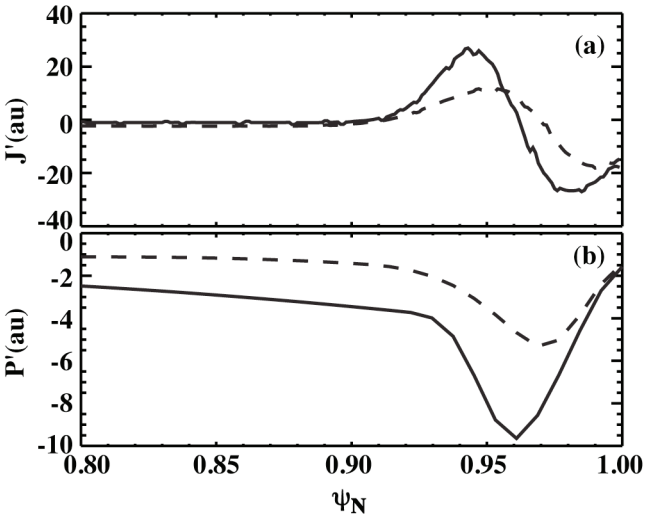

FIG. 3. Reduction in (a) current gradients and (b) pressure gradients before (solid line) and after (dashed line) RMP at 2500 ms [21].

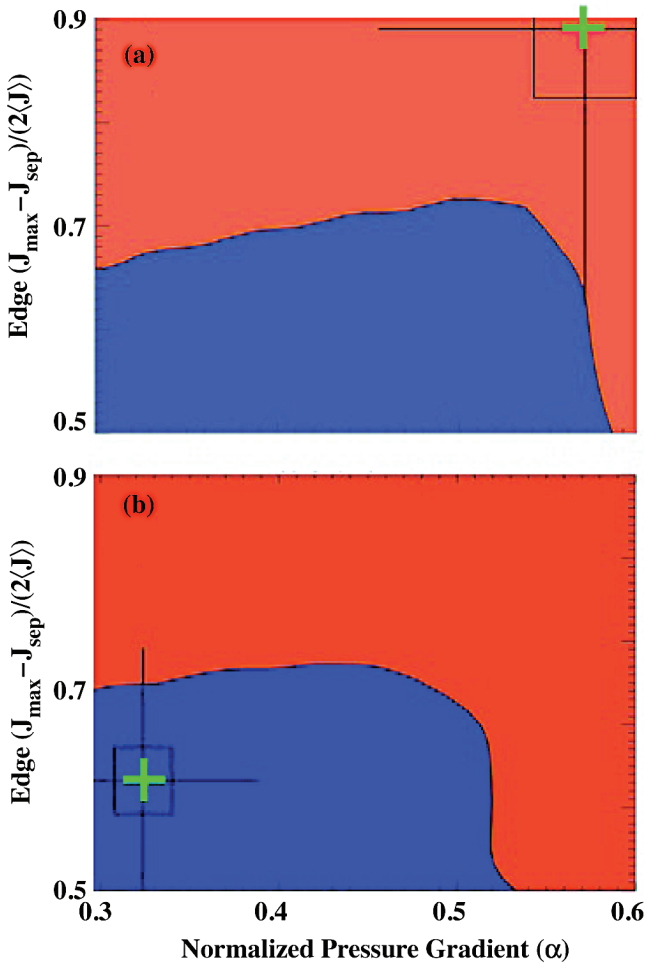

FIG. 4. Peeling-ballooning stability (a) prior to RMP, and (b) during RMP. The red region indicates the locations in α and J' space where at least one toroidal mode has a positive growth rate, whereas the blue region is stable. The experimental operating point is shown by the crosshair [21].

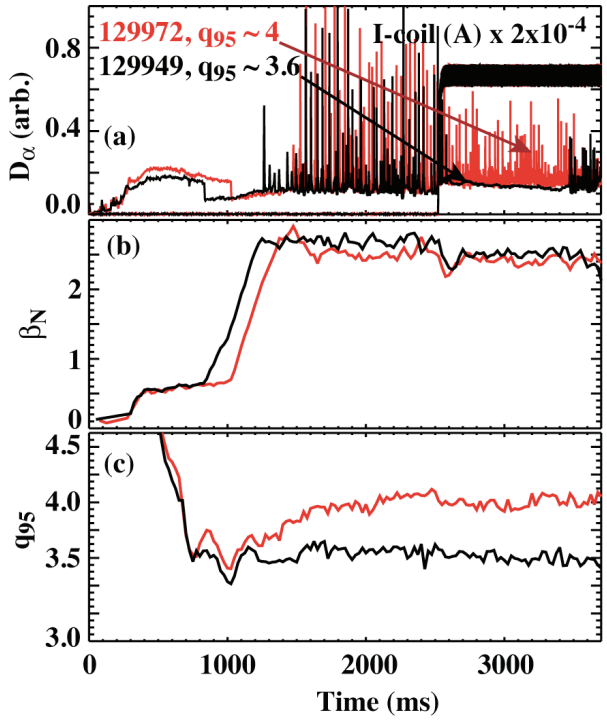

FIG. 5. ELM suppression vs. q_{95}. (a) D_α emission showing ELMs. (b) Line-averaged electron density. (c) β_N. (d) q_{95} [21].

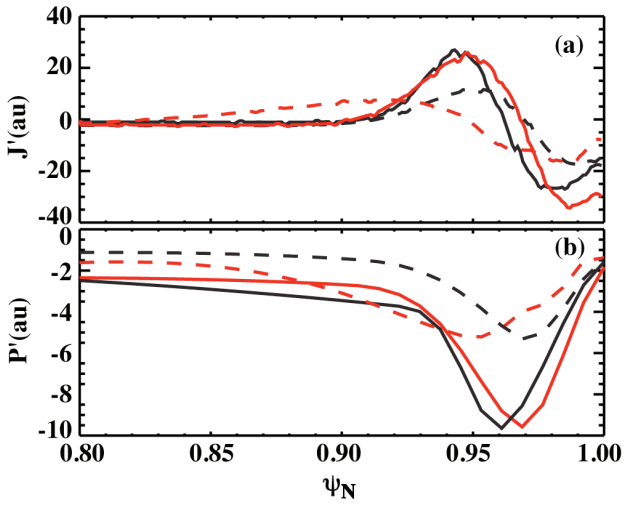

FIG. 6. (a) Current gradient and (b) pressure gradient for two discharges with different q_{95} values (3.6 in black, 4.1 in red/gray), before (solid) and after (dashed) RMP is applied [21].

larger than the q_{95} = 3.6 case. The resulting ELITE calculations, shown in Fig. 7(a,b), for q_{95} = 3.6 case and q_{95} = 4.1 respectively, show that the plasma is P-B stable in both cases. If the P-B model is correct, this implies that the ELMs present during RMP when q_{95} = 4.1 are not Type I ELMs, but instead smaller ELMs (perhaps Type III). The small ELMs that remained when q_{95} = 4.1 have approximately one-third the amplitude (as measured by the D_α emission) and twice the frequency as the large ELMs preceding RMP. The exact classification of the ELMs remains unknown as NBI power scans and fast plasma stored energy loss calculations were not available.

EPED1 was used to calculate the pedestal height vs. q_{95} in both discharges, before and after RMP was applied. EPED1 takes the limits of pressure and edge current used in the ELITE model and incorporates an empirical scaling relating the maximum poloidal beta to the pedestal width characterized by the onset of a kink-ballooning instability. With these constraints, the code determines the maximum pedestal height in an ELMing H-mode plasma. In Fig. 8, the experimental pedestal height (diamonds) is compared to the prediction from EPED1 (triangles). The values of EPED1 for the fiducial cases of an ELMing plasma without RMP were found to be systematically lower than experiment. The predictions presented here are scaled upward by 11%, which is within the error of the model (13%), enabling a more direct comparison to times with RMP. The black symbols denote no RMP, red/gray symbols are during RMP but ELMing, and blue solid symbols are during RMP but without ELMs. After scaling, the predictions of the pedestal height by EPED1 are within the experimental uncertainty of the measured pedestal heights during RMP.

2.4. Effect of q_{95} on Magnetic Confinement

The effectiveness of RMP is predicated on rendering the edge magnetic topology sufficiently stochastic to increase radial transport and reduce pressure and current gradients below the P-B stability limit. For the two hybrid discharges discussed previously, 129949 and 129972,

the q_{95} values are 3.6 and 4.1, respectively. The shot with the higher q did not attain ELM suppression whereas the other did. Here we utilize the TRIP3D [29] field line tracing code to study the difference in the magnetic field line confinement in the two cases. The code does not take into account the plasma response to the applied RMP fields. The code solves the magnetic field line equations, including the external RMP perturbation. 128 field lines are distributed evenly in the poloidal direction on a given magnetic flux surface. The line trajectory is calculated and if a line reaches the vessel boundary it is considered to be 'lost'. In this way, we are able to quantify the field line loss fraction (FLLF) as a function of ψ_N. The length over which field lines are followed was 200 toroidal turns. This length was chosen because the calculated FLLF is asymptotically close to its final value. The FLLF for the two discharges with differing values of q_{95} is shown in Fig. 9. In both cases, the FLLF prior to the application of RMP is very low. During the application of RMP, we see that the shot with q_{95}=3.6 has a higher FLLF than the shot with q_{95}=4.1. The change in the q-profile from q_{95}=3.6 to q_{95}=4.1, served to reduce the effectiveness of the RMP in rendering the edge stochastic and is correlated with the observed lack of ELM suppression.

3. Effect of Bootstrap Current on Magnetic Confinement in High-Beta Discharges

Section 2.4 describes the effects of variations in the magnetic topology on the effectiveness of RMP. Hybrids, and high-beta discharges in general, are characterized by large pressure gradients in the plasma edge. The large pressure gradients drive neoclassical currents, in

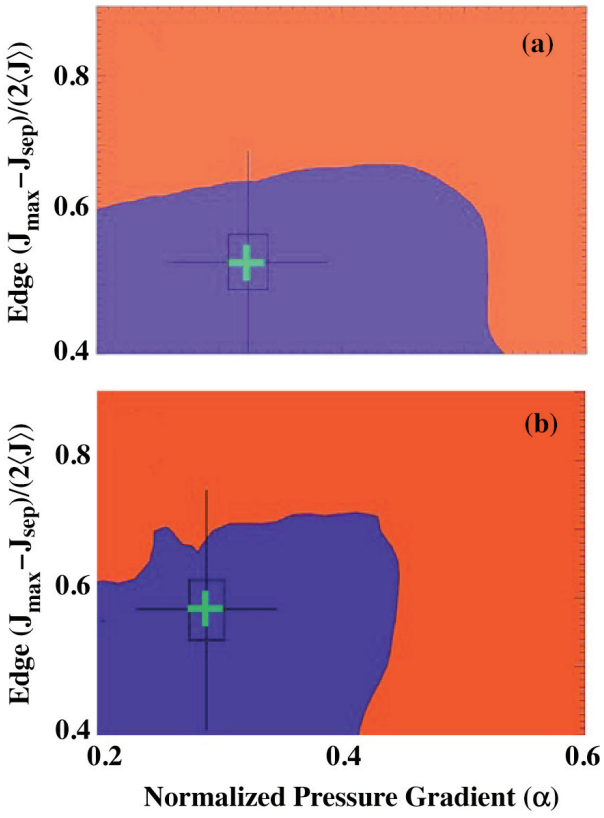

FIG. 7. Peeling-ballooning stability vs. q_{95}. After RMP is applied, both discharges, (a) 129949, q_{95} = 3.6 and (b) 129972, q_{95} = 4.1, are stable to peeling-ballooning modes. The blue and red regions indicate where in α, J' space the plasma would be stable and unstable, respectively [21].

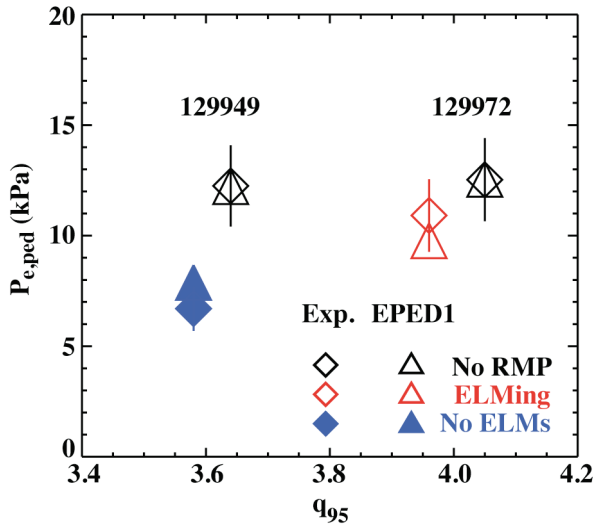

FIG. 8. Pedestal height vs. q_{95}. The experimental pedestal electron pressure (diamonds) and the prediction from the EPED1 model (triangles). Discharges prior to RMP are black symbols, ELMing discharges are shown as red/gray open symbols and ELM suppressed in blue/gray solid symbols. EPED1 data was scaled by a factor of 1.11 to compensate for a systematic offset for the fiducial cases before RMP [21].

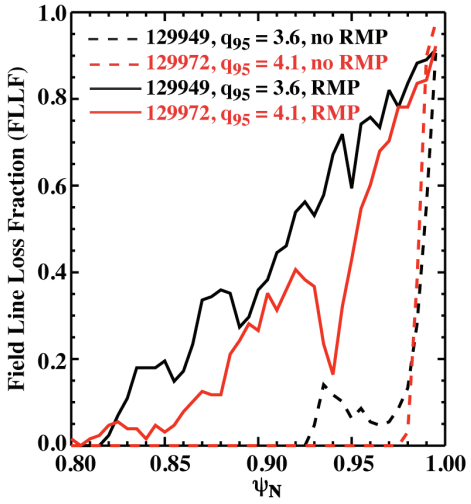

FIG. 9. Field line loss fraction vs. q_{95}. Fraction of field lines reaching the wall prior to RMP (dashed) and during RMP (solid). The loss fraction is higher when q_{95} is 3.6 (black) compared to 4.1 (red).

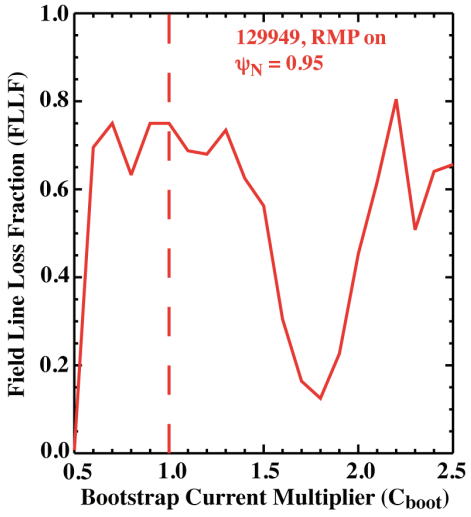

FIG. 10. Field line loss fraction vs. edge current multiplier. Experimental value is at C_{boot} = 1 (vertical dashed)

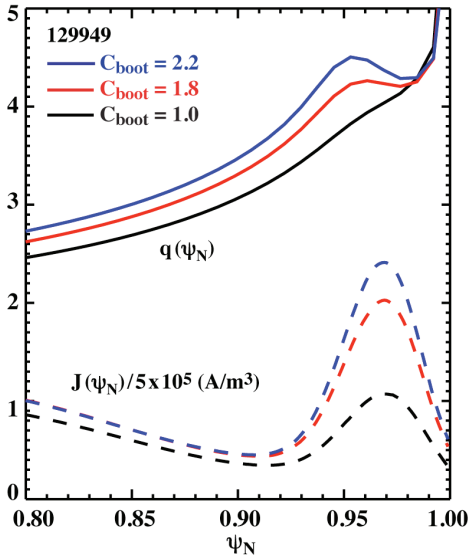

FIG. 11. Effect of edge current on q-profile. Edge current densities (dashed) for values of C_{boot} = 1.0 (black), 1.8 (red), 2.2 (blue). The corresponding q-profiles (solid) are shown.

particular the bootstrap current. The presence of significant toroidal current density in the edge generates a poloidal magnetic field that serves to alter the field line pitch, q. To understand the effects of these currents on RMP ELM suppression, it is instructive to isolate the effect of the bootstrap current from other changes in the plasma, such as the pressure gradient effects, which through the Shafranov shift compress the magnetic surfaces. In performing the ELITE stability analysis for 129949 equilibria were constructed that spanned the P', J' space. By taking the set of equilibria where P' was held to be constant and only J' varied, we can analyze the magnetic topology changes due only to changes in the bootstrap current. The results from the TRIP3D code to generate FLLFs for the differing bootstrap current values are shown in Fig. 10. The edge current profile for the equilibrium generated for 129949 during RMP is multiplied by a scalar C_{boot}. The FLLF is plotted against C_{boot}, at $\psi_N = 0.95$, and we see that the FLLF falls off starting at $C_{boot} = 1.4$ and reaches a minimum at $C_{boot} = 1.8$ before returning to initial fraction of around 2.2. This substantial drop in the FLLF suggests that it would be difficult to attain ELM suppression in this region, though at high bootstrap current, RMP should perform as for lower bootstrap current. The reason for the minima occurring is illustrated in Fig. 11, which plots q and J for several different values of C_{boot}. When the minimum is reached, the q-profile has become quite flat in the edge due to the distortion from the poloidal field generated by the bootstrap current. This serves to separate the magnetic resonances to the point where the island overlap is weak. At higher currents the flat q-profile evolves to a non-monotonic structure that supports a single resonance at multiple ψ_N locations, and stochasticity returns.

4. Conclusions

The application of resonant magnetic perturbation in high-performance plasmas, the "hybrid" scenario, in DIII-D with β_N up to 2.5. The characteristics of complete ELM suppression demonstrated in hybrid discharges, such as dependence on q_{95}, were found to be similar to standard H-mode discharges. This motivates attempting RMP in Advanced-Tokamak (AT) regimes, as would be needed in next-step devices. Using the Sauter bootstrap current model to describe the current density in the edge of these hybrid discharges, and combined with the measured pressure gradient, we are able to study P-B stability during RMP. During periods of RMP ELM suppression, the hybrids, as with standard H-mode plasmas, were stable to P-B modes. The level of magnetic stochasticity imposed by RMP was lower in a high-beta hybrid discharge where q_{95} was outside of the empirical resonance window; the change in magnetic geometry was sufficient to reduce island overlap and field line loss. The FLLF is dependent upon the magnetic shear in the edge, which is strongly influenced by the edge bootstrap current, with the highest FLLF occurring at low/high values of the bootstrap current.

This work was supported by the US Department of Energy under DE-AC05-06OR23100, DE-FC02-04ER54698, and DE-FG03-95ER54309.

References

[1] EVANS, T.E., et al., Phys. Rev. Lett. **92**, 235003 (2004).
[2] BURRELL, K.H., et al., Plasma Phys. Control. Fusion **47**, B37 (2005).
[3] EVANS, T.E., et al., Nucl. Fusion **45**, 595-607 (2005).
[4] MOYER, R.A., et al., Phys. Plasmas **12**, 056119 (2005).
[5] EVANS, T.E., et al., Phys. Plasmas **13**, 056121 (2006).
[6] EVANS, T.E., et al., Nucl. Fusion **48**, 024002 (2008).
[7] FENSTERMACHER, et al., Nucl. Fusion **48** 122001 (2008).
[8] ZOHM, H., Plasma Phys. Controlled Fusion **38**, 105 (1996).
[9] LUCE, T.C., et al., Nucl. Fusion **41**, 1585 (2001).
[10] WADE, M.R., et al., Phys. Plasmas **8**, 2208 (2001).
[11] AYMAR, R., BARABASCHI, P., and SHIMOMURA, Y., Plasma Phys. Controlled Fusion **44**, 519 (2002).
[12] TAYLOR, T.S., Plasma Phys. Controlled Fusion **39**, B47 (1997).
[13] von GOELER, S., STODIE, W., and SAUTHOFF, N., Phys. Rev. Lett. **33**, 1201 (1974).
[14] KADOMTSEV, B.B., Sov. J. Plasma Phys. **1**, 389 (1975).
[15] CONNOR, J.W., et al., Phys. Plasmas **5**, 2687 (1998).
[16] SNYDER, P.B., et al., Phys. Plasmas **9**, 2037 (2002).
[17] BICKERTON, R.J. et al., Nature (London), Phys. Sci. **229**, 110 (1971).
[18] GALEEV, A.A., Zh. Eksp. Teor. Fiz. **59**, 1378 (1970).
[19] GALEEV, A.A., Sov. Phys. JETP **32**, 752 (1971).
[20] PETTY, C.C., et al., Nucl. Fusion **50**, 022002 (2010).
[21] HUDSON, B, et al., Nucl. Fusion **50**, 045006 (2010).
[22] JACKSON, G.L., et al., Controlled Fusion and Plasma Physics 2003 (Proc. 30th EPS Conf. St. Petersburg, 2003) (European Physical Society) P-4.47, http://epsppd.epfl.ch/StPetersburg/PDF/P4_047.PDF
[23] EVANS, T.E., and MOYER, R.A., J. Nucl. Mater. **313-316**, 1282 (2003).
[24] BROOKS, N.H., et al., Rev. Sci. Instrum. **79**, 10F330 (2008).
[25] SNYDER, P.B., et al., Nucl. Fusion **44**, 320 (2004).
[26] CARLSTROM, T., et al., Rev. Sci. Instrum. **63**, 4901 (1992).
[27] RAYMOND, P., et al., Rev. Sci. Instrum. **57**, 2012 (1986).
[28] St. JOHN, H., TAYLOR, T.S. and LIN-LIU, Y.R., Plasma Physics and Cont. Nuclear Fusion Research 1995 (Proc. 15th Intl. Conf. Seville, 1994) (Vienna: IAEA).
[29] EVANS, T.E., MOYER, R.A. and MONAT, P., Phys. Plasmas **3**, 4957 (2002).